Applied Surface Science 557 (2021) 149795

Contents lists available at ScienceDirect

Applied Surface Science

journal homepage: www.elsevier.com/locate/apsusc

Full Length Article

Towards prevention of biofilm formation: Ti6Al7Nb modified with nanocomposite layers of chitosan and Ag/Au nanoparticles

K. Kleszcz [a], M. Hebda [b], A. Kyzioł [c], H. Krawiec [d], K. Kyzioł [a,*]

[a] Faculty of Materials Science and Ceramics, AGH University of Science and Technology, A.Mickiewicza Av. 30, 30 059 Kraków, Poland
[b] Faculty of Materials Engineering and Physics, Cracow University of Technology, Warszawska 24, 31 155 Kraków, Poland
[c] Faculty of Chemistry, Jagiellonian University, Gronostajowa 2, 30 387 Kraków, Poland
[d] Faculty of Foundry Engineering, AGH University of Science and Technology, Reymonta 23, 30 059 Kraków, Poland

ARTICLE INFO

Keywords:
Biopolymers
Gold nanoparticles
Silver nanoparticles
Ti6Al7Nb alloy
Biocompatibility

ABSTRACT

Implant-associated infections are the major concern for failure of arthroplasty operations. The functionalisation of implant surface can provide solutions to the problem by either inhibiting the adherence of the bacteria or introducing a contact-killing mechanism. This work is focused on Ti6Al7Nb biomedical alloy modification involving chemical and plasma surface activation, followed by the deposition of chitosan layers enhanced with metal nanoparticles. A benign method using chitosan as an efficient reducing and stabilizing agent was applied to produce Au and Ag nanoparticles in situ with the size of ca. 20 nm and 5 nm, respectively. Piranha solution and O_2/NH_3/Ar plasma were used as a surface activation method, while Au and Ag NPs provide antimicrobial properties, as a viable alternative to the antibiotic-based approach. The surface topography on submicrometre scale of deposited layers was evaluated. Chitosan and chitosan–Ag NPs composite layers showed excellent hydrophilicity, characterised by wetting angles below 13°. Modified alloy showed minimal toxicity towards MG-63 cell line *in vitro*, acceptable corrosion resistance and release of titanium, aluminium as well as niobium ions from the resulting modified alloys. The chitosan layers were proven to uphold satisfactory Au (over 2.8 mg/dm^3) and Ag (over 5.1 mg/dm^3) ion dosages up to 96h.

1. Introduction

The amount of arthroplasty operations in recent decades, including total hip replacement procedures, has increased significantly and is projected to rise in the future by various estimates [1–3]. The leading causes of such trends being mainly the wider availability of specialised medical care, increased life expectancy, rise in obesity rates and ageing population of first word countries. Given such circumstances, the increase in value of global biomaterial market, including metallic implant sector, is expected. Among metallic biomaterials, titanium and titanium alloys possess several desirable traits. For example: biocompatibility, low Young's modulus, corrosion resistance, fatigue resistance, which justify its widespread usage in clinical practice. This popularity is reflected by numerous research concerned with technology and modification of titanium-based alloys, which are focused on solving existing issues with medical usage of this particular group of materials. One such problem revolves around appropriate choice of alloying elements, in regards to biocompatibility of implant and its long term usage. Studies focused on harmful influence of vanadium atoms on human tissue, have put under consideration usage of popular alloy such as Ti6Al4V [4–6]. The need to replace vanadium has led to development of alloys such as NiTi, Ti15Zr4Nb4Ta, Ti13Nb11Zr, and especially Ti6Al7Nb, which offers similar properties and manufacturing costs to Ti6Al4V [7]. The continuous effort to reduce potentially harmful additions is likely to be preserved, as suspicion towards long term exposure to aluminium ions, its effect on human body and contribution to neurological diseases grow in the academic field [8].

In addition to improving the bulk material itself, surface engineering plays an important role in the development of safe and effective medical devices, as for the most part organism reaction to implant is dependent on material-tissue interface [9]. Besides surface modifications and coatings improving biocompatibility, osteoblast proliferation, differentiation and bone integration, the topic of antibacterial coatings is emerging trend in recent scientific literature. Implant-associated infections are still the leading cause of implant failure, putting patients health in danger and straining healthcare funds by generating additional

* Corresponding author at: AGH University of Science and Technology, Faculty of Materials Science and Ceramics, 30-059 Kraków, Poland.
E-mail address: kyziol@agh.edu.pl (K. Kyzioł).

https://doi.org/10.1016/j.apsusc.2021.149795
Received 20 November 2020; Received in revised form 6 April 2021; Accepted 7 April 2021
Available online 14 April 2021

costs due to treatment and additional surgeries [10]. Moreover, the rising problem of antibiotic resistant bacteria adds complexity in finding proper solution against bacterial colonisation of implant surface. Research shows, that the very problem is best tackled at the initial phase of bacterial adhesion before biofilm that consists of polymerized polysaccharides starts forming, which significantly reduces the effectiveness of antimicrobial agents [11]. Therefore, the current approach of surface functionalisation focuses on either reducing bacteria adhesion or introducing a contact killing mechanism [12,13]. The former is achieved by controlling physiochemical parameters such as surface energy, wettability or surface charge by means of creating appropriate chemistry, topography and controlled feature size [14]. Such nano- and microstructures include, but are not limited to, nanorough surfaces [15], titania nanopillars [16] and nanowires [17], charged polycation biopolymer layers [18] or polymeric brushes [19,20]. Those modifications significantly reduce bacterial adhesion, while not inhibiting cell growth. To attain bactericidal effect similar topographical features, with strictly controlled dimensions, can be used to induce bacterial cell lysis [17]. The exact patterns are often inspired by naturally occurring structures, emphasizing biomimetic approach in biomaterials science [21]. Another approach utilizes bactericidal agents introduced in forms of layers, nanoparticles and substances anchored or embedded into surface. Besides antibiotics such as minocycline [22], ciprofloxacin [23] or vancomycin [24] alternatives such as antimicrobial peptides [25], biopolymers [26], metallic ions and nanoparticles [27–34] are gaining popularity.

In particular, usage of metal nanoparticles has been extensively studied in current literature, providing wide variety of synthesis methods, including physical methods [35], wet chemistry [36] and so called green chemistry methods [37–40] yielding mono–, bi– or even trimetallic structures [40]. Due to their extraordinary properties they found a multitude of applications, ranging from catalysis [41,42], sensors [43] to cancer treatment [44]. Moreover, their antibacterial properties are highly applicable in areas such as the food industry [45], textile industry [39] and biomedical use [29]. It is agreed upon, that the introduction of noble metals ions and nanoparticles into surface composition provides satisfactory antibacterial effect while having minimal toxicological effect on surrounding cells, provided sufficiently small concentration. Unlike modifications utilizing antibiotics, usage of agents such as gold or silver in form of ions and nanoparticles (NPs) can bypass defences of antibiotic-resistant bacteria, which adds to the attractiveness of such solutions. Current approach presents wide variety of ways to immobilise NPs including entrapment in pores [30], electrostatic attraction or chemical binding to functionalised surface *via* organic moieties [28]. The development of herein described ideas paves the way to new generation of medical implants or devices, capable of fighting off bacterial invasion.

In this work the novel multi-step approach to Ti6Al7Nb alloy modification is proposed, consisting of chemical etching, plasma etching and deposition of chitosan layers with Au NPs/Ag NPs. The active surface of proper topography and chemistry was achieved by chemical and plasma treatment. Simple chitosan deposition *via* immersion, coupled with in situ chitosan-mediated synthesis of Au NPs or Ag NPs provides easy way of biomedical alloy functionalisation. Such procedure was developed in order to elicit positive host body reaction and improved bone integration, while introducing antibacterial effect. Successful deposition of nanoparticles embedded in biopolymer matrix was proven and the effect of layers on medical alloy characteristics, such as static contact angle, corrosion current or ion release profiles was measured. Additionally, a quantitative study to determine changes in the mechanical parameters of the surface using the nanoindentation method was carried out.

Thus, the main goals of this study were to: (1) develop a relatively simple, yet effective surface modification technology preventing biofilm formation, promoting osteointegration, providing corrosion resistance and diffusion barrier for metal ions, (*2*) characterise physiochemical state of surface after undergoing proposed treatment, (*3*) evaluate biological response *in vitro*, paying special attention to possible toxicological effects of silver and gold ions, (*4*) characterise mechanical properties of deposited layers, and (*5*) compare features and biological responses of investigated surface modifications on different stages.

2. Materials and methods

2.1. Sample preparation and surface treatment

Rod of Ti6Al7Nb alloy (diameter 16 mm, Shaanxi Yunzhong Industry Development) was cut into discs, 4 mm thick each. In order to remove natural oxide layers, clean and prepare surface for next steps of surface modification, each sample was manually ground using SiC grinding paper (grits: #180, #320, #500, #800, #1000, #1200, Struers) and polished using diamond pastes of grain size 9 μm (DiaPro Allegro, Struers), 3 μm (DiaPro Dac, Struers) and 1 μm (DiaPro Nap B, Struers) until mirror polish was achieved.

Prior to experiment samples were divided into five experimental series and functionalized accordingly:

1) Non-modified reference samples – L0
2) Chemically etched, plasma modified samples – L1
3) Chemically etched, plasma modified, chitosan deposited samples – L2
4) Chemically etched, plasma modified, chitosan + Au NPs deposited samples – L3
5) Chemically etched, plasma modified, chitosan + Ag NPs deposited samples – L4

Chemical etching was conducted in Piranha solution containing 40% NH_3OH solution, 30% H_2O_2 solution and deionized water in volume ratio of 1:1:5. Each batch was submerged for 20 min. at constant temperature of 70°C. Immediately after etching samples were rinsed in NaOH solution and deionized water multiple times.

The plasma treatment was carried out in low pressure conditions (0.8 Tr) in RF CVD system (13.56 MHz, Elettrorava S.p.A., Turin, Italy), under the constant flow of gases: O_2 (50 sccm), NH_3 (45 sccm), Ar (5 sccm) for 60 min. Process was performed under ambient temperature and set power density of 0.6 W/cm^2.

Biopolymer solutions were prepared by dissolution of chitosan (CS) of average molecular weight of 1278 ± 8 kDa in 0.1 M acetic acid, process was conducted in oil bath, at a temperature of 65 °C under stirring for 12 h. Au NPs were obtained by controlled reduction of $HAuCl_4$ (5 mM) by CS (1% (w/v)) in volumetric ratio $HAuCl_4$:CS of 5:2 [32]. While, Ag NPs were formed by concomitant reduction of $AgNO_3$ (52 mM) by both CS (1% (w/v)) and ascorbic acid (Vit.C, 1 mM) as reductants in volumetric ratio $AgNO_3$:CS:Vit.C of 1:5:1 [33]. The successful incorporation of gold and silver NPs were confirmed by UV–VIS spectroscopy (Fig. S1, Supplementary Material). Chitosan-based layers were prepared by the solvent evaporation method. Layers were deposited on plasma pre-activated Ti6Al7Nb substrates by immersion in prepared CS solutions, diluted by deionized water (the volumetric proportions CS:dH_2O were: 1:6 for L2 series and 1:4 for L3 and L4 series) for 30 min, under gentle rocking motion. After deposition each sample was rinsed in 4% NaOH solution and deionized water multiple times.

2.2. Physicochemical surface characteristics

2.2.1. Microscopic observation

Surface structure investigation was performed using SEM microscope (Nova NANO SEM 200) after layers were deposited as well as after corrosion behavior measurements. Transmission electron microscope equipped with a cryo-holder station (FEI Tecnai T20 microscope) was used to examine the morphology of the synthesized Ag and Au nanoparticles obtained in the parent silver- or gold–chitosan dispersions and

to examine their distribution in the cast films. The size distribution of nanoparticles was determined from the enlarged TEM micrographs, using commercially available software ImageJ, counting at least 200 particles in different images. Topography of obtained surfaces was evaluated using optical profilometer (Leica L series), arithmetical mean height (S_a) and root mean square height (S_q) were collected over three scans of different areas (350.88 × 264.19 μm) for each sample series. In addition, the thickness of the obtained layers was determined using optical profilometry (Alpha Step IQ, KLA-Tencor Corp., Milpitas, CA, USA), based on selected micro-area of the tested samples.

2.2.2. Chemical characterization

To ensure proper chemical composition of deposited layers EDS (EDAX GENESIS) measurements were conducted. Samples coverage by chitosan layers was checked by Fourier–transform infrared spectroscopy (BIO-RAD FTS6000), using Attenuated Total Reflectance method (FTIR).

2.2.3. Contact angle measurements

The static contact angles and free surface energy were assessed for all series by contact angle measurements (Kruss DSA25E) *via* sessile drop technique, utilizing diiodomethane and deionized water. Measurements were repeated fivefold for each series and conducted under ambient conditions, free surface energies were calculated using OWRK (Owens-Wendt-Rabel-Kaelble) model.

2.2.4. Voltammetry study

Corrosion behavior of modified surfaces was assessed using linear sweep voltammetry method, utilizing surveyed sample as working electrode, silver chloride electrode as reference and platinum auxiliary electrode. Ringer solution (8.6 g/L NaCl, 0.3 g/L KCl, 0.243 g/L $CaCl_2$, pH = 7.15 ÷ 7.30) under constant temperature of 37°C, simulating body fluid conditions, was used as electrolyte. In each case sweep was made from +1.5 V to −1.0 V with linear step of 0.001 V/s using potentiostat/galvanostat (Autolab PGSTAT128N, Metrohm).

2.2.5. Mechanical testing

Hardness and Young's modulus of deposited layers were estimated using nanoindenter (Anton Paar), basic tribological information were collected by means of scratch testing as well. The nanoindentation was performed using diamond Vickers indenter, in low (20, 30, 40, 50 mN) and high (200, 400, 600, 800 mN) load regime with loading speed equal twice the total load value, expressed in mN/min. Hardness and Young's modulus were calculated according to Oliver-Pharr method [46]. The resistance to scratches in the micro-scale was evaluated using a scratch test (MST3, Anton Paar). During the measurement, the load of the Rockwell-type diamond indenter (radius: 100 μm) increased in a linear manner from 0.03N up to 5N, at a rate of 1.99 N/min, the test was carried out on a 5 mm distance.

2.2.6. Evaluation of biological activity

To address potential cytotoxicity, a series of *in vitro* experiments were conducted on MG-63 cell line. Alamar Blue assay (Sigma-Aldrich) was carried out after 48h and 96h as follows: cells were cultured in Dulbecco's Modified Eagle Medium – DMEM (Immuniq, Poland), supplemented with phenol red, 10% fetal bovine serum (FBS) and 1% of streptomycin/penicillin (Gibco-BRL, Life Technologies, Germany). After UV light sterilisation (20 min), samples were placed in sterile 24-well culture plate and surface was seeded with 0.2 ml of cell suspension ($50x10^4$ cells). As a control, cells were cultivated on bare culture plates (negative control, Corning Inc., USA). Medium was changed every 24h for a fresh one. After appropriate time has passed, Alamar Blue assay was carried out according to the well-known protocol [47]. Cellular metabolic activity was monitored with application of multimode microplate reader (Infinite 200 M PRO NanoQuant, Tecan, Switzerland), using 605 nm wavelength (excitation wavelength 560 nm). Cytotoxicity was expressed as a percentage of viable cells in relation to control. Additionally, cell populations harvested from the samples were analyzed by flow cytometry (BD FACSCalibur™, BD Bioscience), using Annexin-V-FITC (Apoptosis Detection Kit; Invitrogen) to detect early and late apoptosis, while 7-AAD (7-Amino-Actinomycin D) (Viability Staining Solution; eBioscience Reagents, Thermo Fisher Scientific) to stain necrotic cells. Moreover, samples of a growth medium from the cell cultures being treated (Alamar Blue assay after 48h and 96h) were collected and analyzed by means of inductively coupled plasma mass spectrometry (ICP-MS) in order to measure the concentration of released ions (Elan 6100 Spectrometer).

3. Results and discussion

3.1. SEM observations, profilometer investigation and layer chemistry investigation

Surface microstructure investigation, using SEM microscopy, was carried out to observe topographical changes after each applied modification (Fig. 1). The change of the surfaces microstructure after subsequent modifications can be clearly observed as smooth titanium surface (Fig. 1, L0), however appears to be more developed after chemical etching and plasma treatment (Fig. 1, L1). Chitosan-based layers (Fig. 1, L2–L4) seem to appear even rougher than previous surfaces, although the topography of island-like pure CS layer differs from those containing nanoparticles, having more homogenous structure. To acquire more information about chemical nature of surface and confirm deposition of planned layers, EDS scans of SEM micrographs were made (Table 1).

It can be noticed that etching in Piranha solution and usage of oxygen containing plasma increased overall oxygen content, related to TiO_2 layer growth, compared to unmodified titanium alloy. As expected, immersion in chitosan solution caused elevated oxygen content and appearance of carbon peak, likely related to chitosan. Moreover, in the case of surfaces enriched with metal nanoparticles gold and silver content, respectively were detected in L3 and L4 sample series, respectively.

To get an insight into the uniformity of the AuNPs distribution among the nanocomposites, TEM analysis of the thin films, previously casted on plastic substrates, was used to assess the shape and size distribution of the as-prepared nanoparticles (Fig. 2).

Microscopic visualization revealed the formation of mainly spherical shaped silver or gold particles. Statistical analysis of the NP sizes based on the obtained micrographs (inserts) allowed to determine the size of 16 ± 5 nm and 8 ± 3 nm for Au NPs and Ag NPs, respectively.

Then, to identify possible interactions between silver or gold nanoparticles and chitosan molecules FTIR measurements were carried out. FTIR spectra of chitosan, chitosan-Au NPs, and chitosan–Ag NPs films are presented in Fig. 3.

Typical FTIR spectra of chitosan present representative peaks at ~1640 and ~1550 cm^{-1} related to amide groups, *i.e.* acetylated amine, and to free amine groups (*i.e.* deacetylated amine) [48], respectively. Distinctive peaks originating from glyosidic ring (1018 cm^{-1} and 1060 cm^{-1} peaks), CH_2 wagging (1320 cm^{-1}), —CH_3 symmetric deformation (1377 cm^{-1}) and wide band, consisting of overlapping peaks, related to NH and OH stretching (3255 cm^{-1}) can be observed [49]. Moreover, less intensive peaks were detected at 650 cm^{-1} (OCO vibrational mode of acetic acid) [49], 893 cm^{-1} (CH alkene stretching), 1155 cm^{-1} (CO stretching), 2876 cm^{-1} and 2930 cm^{-1} (symmetric and asymmetric CH stretching) [34]. The most characteristic change coming from metal – chitosan interactions is connected with the shift of amino group band (~1550 cm^{-1}) to lower wavenumbers in the presence of metal NPs due to electrostatic interactions between the polymer and the metal. As well, when metals are incorporated in the chitosan films a significant change in the relative intensity of these bands should be observed. The integrated intensity ratio $I_{\sim1550}/I_{\sim1640}$ depends firstly on the molecular weight of the polymer and secondly on metal content. For instance, it was shown that it significantly decreased with silver loading [48].

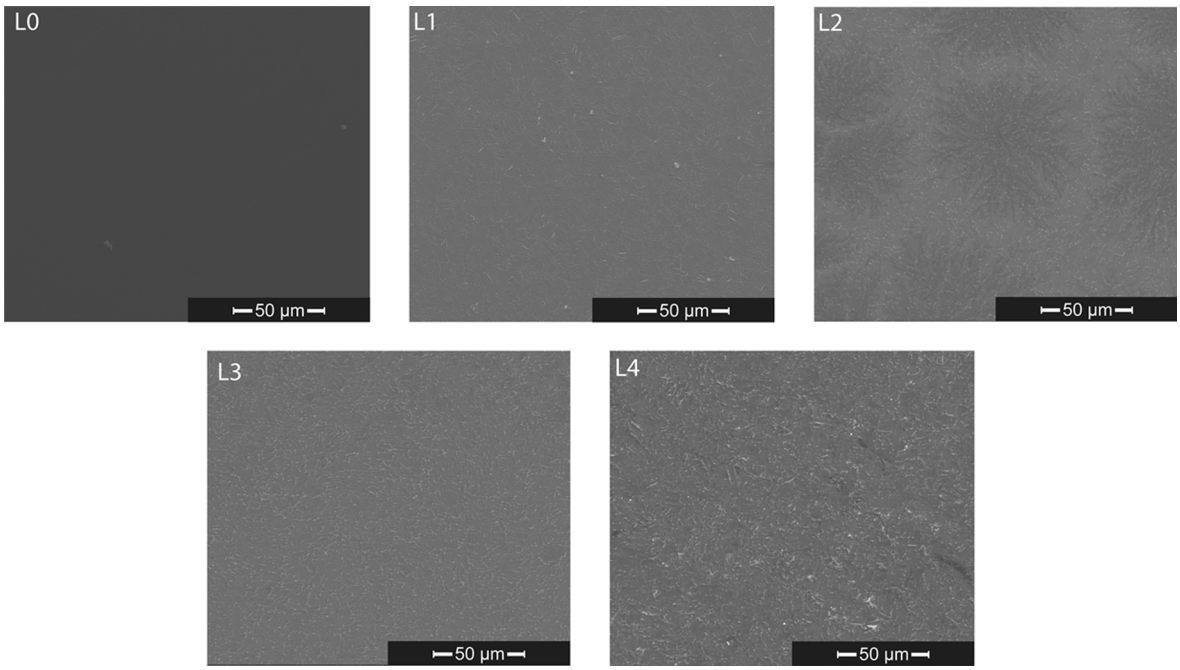

Fig. 1. SEM micrographs of reference sample (L0), sample after chemical and plasma treatment (L1), CS layer (L2), CS/Au NPs layer (L3) and CS/Ag NPs/Vit.C layer (L4).

Table 1
Concentrations of selected elements based on EDS analysis of L0–L4 samples.

Element	Element concentration (wt. %)				
	L0	L1	L2	L3	L4
Ti	84.9 ± 0.1	82.2 ± 0.1	58.8 ± 0.1	76.0 ± 0.1	74.3 ± 0.1
Al	6.0 ± 0.1	5.3 ± 0.1	7.6 ± 0.1	5.3 ± 0.1	4.9 ± 0.1
Nb	6.8 ± 0.1	5.6 ± 0.1	13.1 ± 0.1	6.1 ± 0.1	6.0 ± 0.1
O	2.3 ± 0.1	6.9 ± 0.1	25.7 ± 0.1	7.4 ± 0.1	12.7 ± 0.1
C	–	–	4.8 ± 0.1	1.2 ± 0.1	1.5 ± 0.1
Au	–	–	–	3.9 ± 0.1	–
Ag	–	–	–	–	0.6 ± 0.1

Likewise, it was demonstrated for chitosan when it is chemically cross-linked with other polymers (*e.g.*, with PEG). Thus, the intensity of the band at ~1640 cm^{-1} can be considered as internal [50]. By extension, following Wei and Qian [51] the attachment of silver or gold NPs to nitrogen atoms in chitosan–NPs samples reduces the vibration intensity of the N—H bonds. This would be presumably due to the increase in the molecular weight of the complex that becomes heavier after metal NPs bonding. In the reported study, the decrease in the intensity of the band related to the NH groups in the primary amines in the prepared films supports the hypothesis that silver/gold nanoparticles are interacting with nitrogen atoms of chitosan.

Finally, the changes in roughness of titanium alloy after proposed modifications were analysed by light profilometer (Fig. 4).

Arithmetical mean height (S_a) and root mean square height (S_q) parameters were calculated, based on three independent scans made for each sample (Table 2).

The obtained roughness parameters suggests a drop in overall roughness after etching in Piranha solution and plasma etching took place (L1 sample), compared to unmodified sample (L0). Titanium surface modified with CS and CS/Ag NPs/Vit.C layers (L2 and L4, respectively) shows higher roughness than L1, although not as high as L0. Surprisingly, CS/Au NPs coated sample (L3) roughness exceeded the value calculated for reference sample and is a clear outlier among chitosan-based modifications. The cause of such effect may be related to higher amount of gold nanoparticles incorporated into the layer, as compared to L4 sample (Table 1). Based on conducted analysis the thickness of obtained layers of series L2 (CS), L3 (CS/Au NPs) and L4 (CS/Ag NPs/Vit. C) were *ca.* 1.2 μm, *ca.* 1.0 μm, and *ca.* 0.5 μm, respectively.

As proved by EDS (Table 1) and FTIR (Fig. 3) measurements CS, CS/Au NPs and CS/Ag NPs/Vit.C layers were successfully deposited on Ti6Al7Nb alloy. What is more, in the case of chemically and plasma modified sample (L1) the increased oxygen content, compared to pure titanium alloy, was detected. Thus, treatment with Piranha solution as an etching agent and oxygen containing plasma is largely responsible for this effect. This finding suggests formation of a thicker layer based on titanium oxide, which acts as diffusion barrier for metallic ions and is the reason of inherent corrosion resistance of titanium. The presented results are in agreement with Nazarov *et al.* [52], who also demonstrated such positive effects of chemical etching in basic Piranha solution. This beneficial effect of plasmo-chemical treatment deserves emphasis as it enhances a long term implant performance. The state of the surface has changed significantly after applying proposed modifications, as it was confirmed by SEM observations. The usage of chemical etching with Piranha solution and plasma treatment lead to more developed surface topography (Fig. 1, L1). As light profilometer measurements suggest, the overall roughness of the etched surface was lower, compared to the unmodified state (Table 2). This might be explained by preferential etching at surfaces peaks and valleys, therefore such treatment helped to homogenise surfaces feature size. It is worth noting that according to Solař *et al.* [53] S_q parameter of 30 nm is optimal for MG–63 cell growth. L1 modification was the closest to this value among all measured samples (S_q, 0.0763 ± 0.0095 μm), showing the potential of combined chemical and plasma etching in achieving proper surface parameters in nanoscale. The resulting data as well as previous studies [54] suggest usage of proper plasma treatment in modification of biomaterials in order to create advantageous surface chemistry and topography. On the other hand, the deposition of chitosan layers, regardless of content, contributed to increased roughness. With the exception of L3 sample, the contribution was not big enough to exceed values recorded for reference (L0) sample, what is more the roughness parameters of chitosan layers do not seem to be the deciding factor in subsequent biocompatibility studies performed on MG-63 cell line.

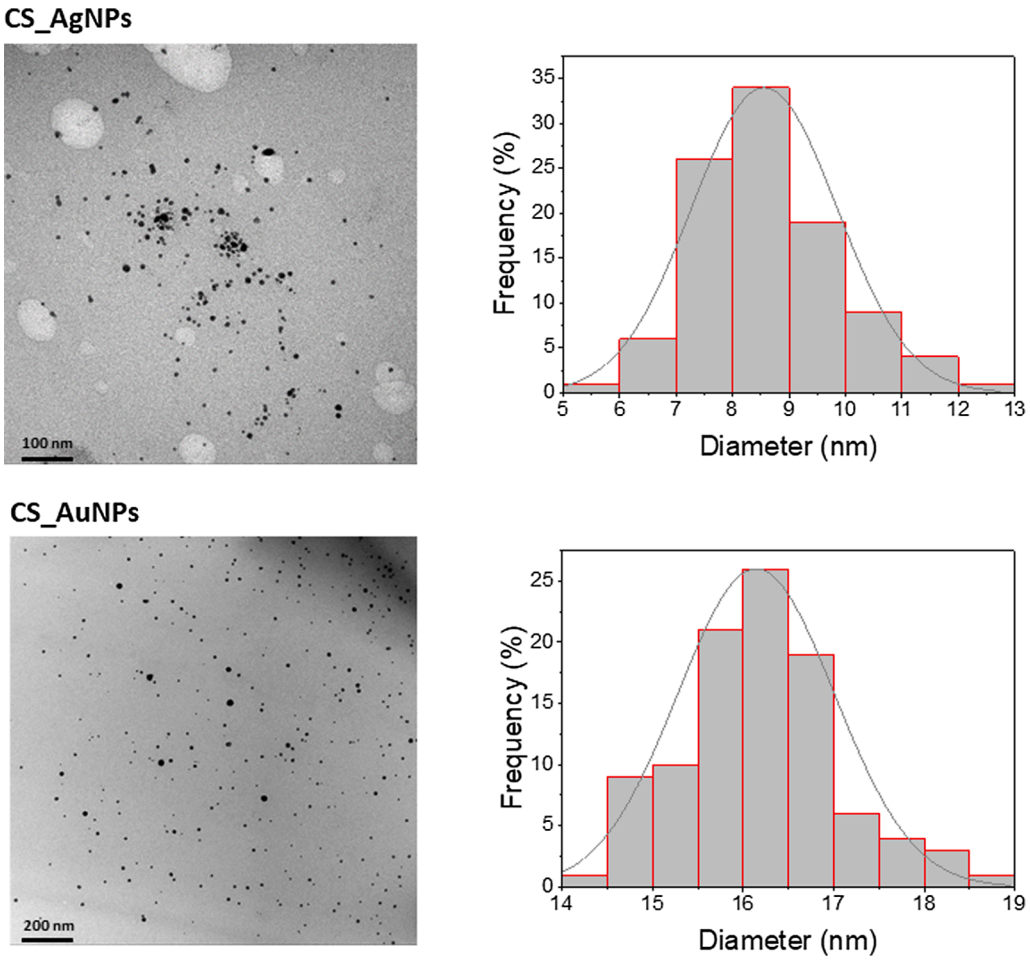

Fig. 2. TEM images of the cast films of CS/Ag NPs/Vit. C and CS/Au NPs. Inserts depict size distribution histograms for Ag and Au nanoparticles, respectively.

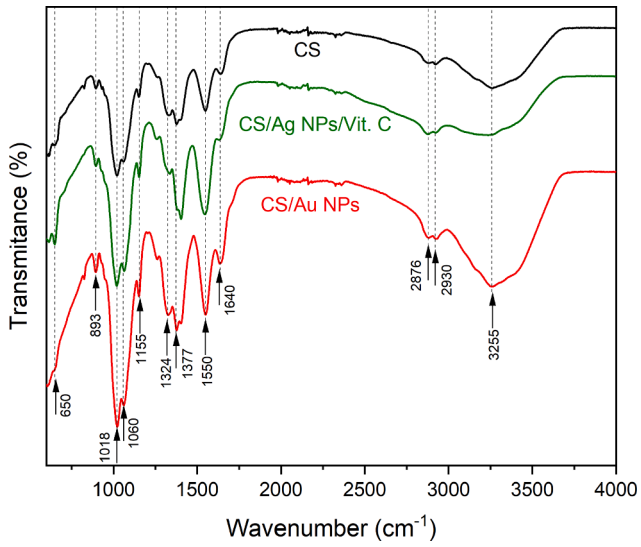

Fig. 3. FTIR-ATR spectra of CS layer (L2), CS/Au NPs layer (L3) and CS/Ag NPs/Vit. C layer (L4).

3.2. Contact angle and surface energy measurement

Fabrication of proper surface wettability is paramount to issues concerning both osteointegration of the implant and its bacteriostatic properties. Contact angle, and therefore surface free energy (SFE), has major implications in regards to early implant integration (*i.e.* protein absorption) as well as bacteria attachment to the surface [55]. Contact angles of deposited layers were measured by sessile drop method, using water and diiodomethane as liquids of choice. Based on results, corresponding SFE together with polar and dispersive parts were determined by OWRK (Owens-Wendt-Rabel-Kaelble) model (Fig. 5).

The slightly hydrophilic character of pure Ti6Al7Nb surface was changed in each of applied surface modification. Following chemical etching in Piranha solution and plasma treatment in O_2/NH_3/Ar atmosphere a shift towards hydrophobic character was observed. On the other hand immersion deposition of CS and CS/Au NPs layers resulted in strongly hydrophilic surface, reaching as low as $11.15 \pm 1.02^{\circ}$ for pure CS layer with CS/Au NPs being a close second ($12.01 \pm 4.35^{\circ}$). Contrary to previous chitosan-based modifications (L2 and L3), CS/Ag NPs/Vit.C layers resulted in only slightly smaller contact angle, in comparison to pure titanium alloy. Likewise, low contact angle was obtained by Zhang *et al.* [56], who used Layer by Layer (LbL) deposition of alternating heparin and chitosan layers. Values as low as 8° were obtained for chitosan terminated composites (heparin/CS), although unlike our study such results were linked to initial alkaline treatment. As Yuan *et al.* [55] points out, extremely low or high contact angle can help in reducing bacteria adhesion, demonstrated on example of *E. coli* strain. However, in that study a polystyrene substrate was used as a surface of choice, preventing direct comparison with obtained CS layers. Calculated SFE show slightly lower energy for Piranha and plasma treated surfaces, compared to control sample (unmodified Ti6Al7Nb alloy). Indeed, in the case of all three chitosan-based layers, obtained SFE values were higher than values for pure alloy sample. SFE investigations also revealed dominating contribution of dispersive part in case of L1 series (chemical

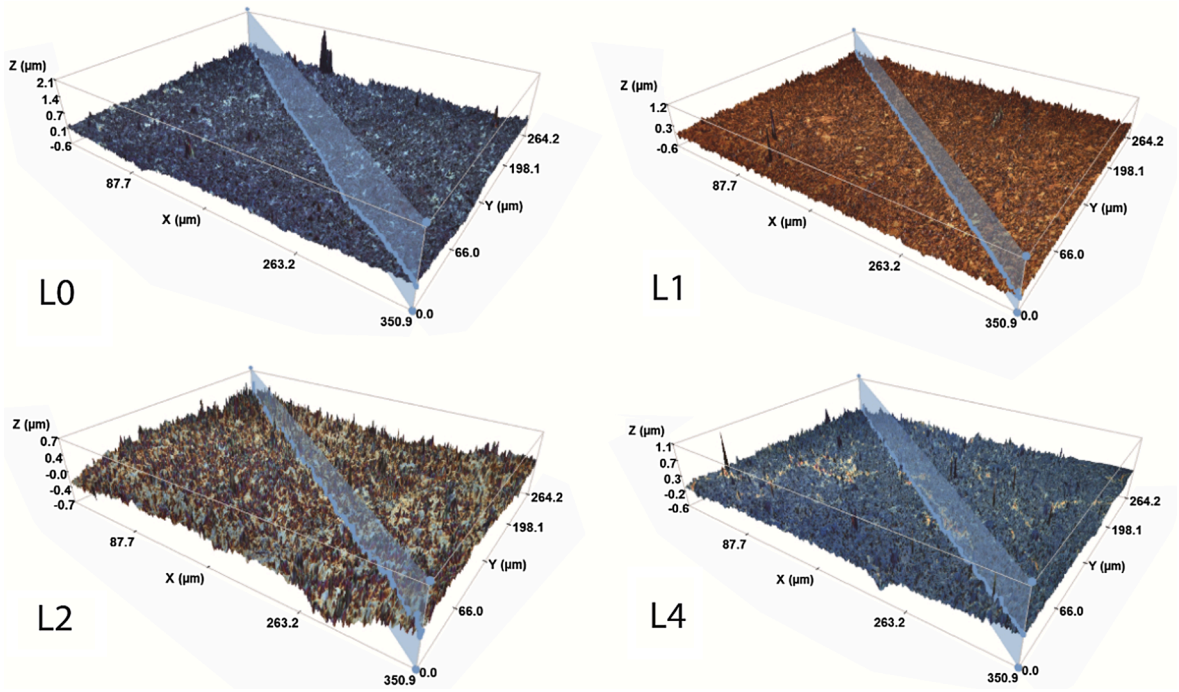

Fig. 4. Selected 3D surface scans of unmodified Ti6Al7Nb alloy (L0), plasma treated sample (L1), pure chitosan layer (L2), and Ag NPs enhanced chitosan layer (L4).

Table 2
Roughness parameters obtained by light profilometer measurements: arithmetical mean height (S_a) and root mean square height (S_q) of L0–L4 samples. Results presented as arithmetical mean ± SD.

Surface parameter	Sample series				
	L0	L1	L2	L3	L4
S_a (µm)	0.0937 ± 0.0167	0.0521 ± 0.0036	0.0865 ± 0.0275	0.1177 ± 0.0550	0.0801 ± 0.0242
S_q (µm)	0.1401 ± 0.0376	0.0763 ± 0.0095	0.1163 ± 0.0316	0.1504 ± 0.0075	0.1189 ± 0.0410

and plasma treatment) and L4 series (CS/Ag NPs/Vit.C). In the case of L2 (pure CS) and L3 (CS/Au NPs) polar interactions were the majority.

3.3. Corrosion study

The influence of applied surface modifications on corrosion behaviour was measured by linear sweep voltammetry (LSV) in Ringer solution, simulating body fluid conditions (Fig. 6).

The reference specimen L0 (Ti6Al7Nb alloy) revealed typical passive behaviour in the Ringer solution. Two current plateau are visible: the first one is visible in the potential range from −0.25V to 0.5V, then the anodic current increases, and the second current plateau is present at the potential above 0.75V (Fig. 6). In the anodic domain, a very low current density (few microampere per square centimetre) is detected. This result confirms that Ti6Al7Nb alloy exhibits high corrosion resistance in the Ringer solution. The data acquired in the case of first three sample series showed both similar corrosion potential and corrosion current density

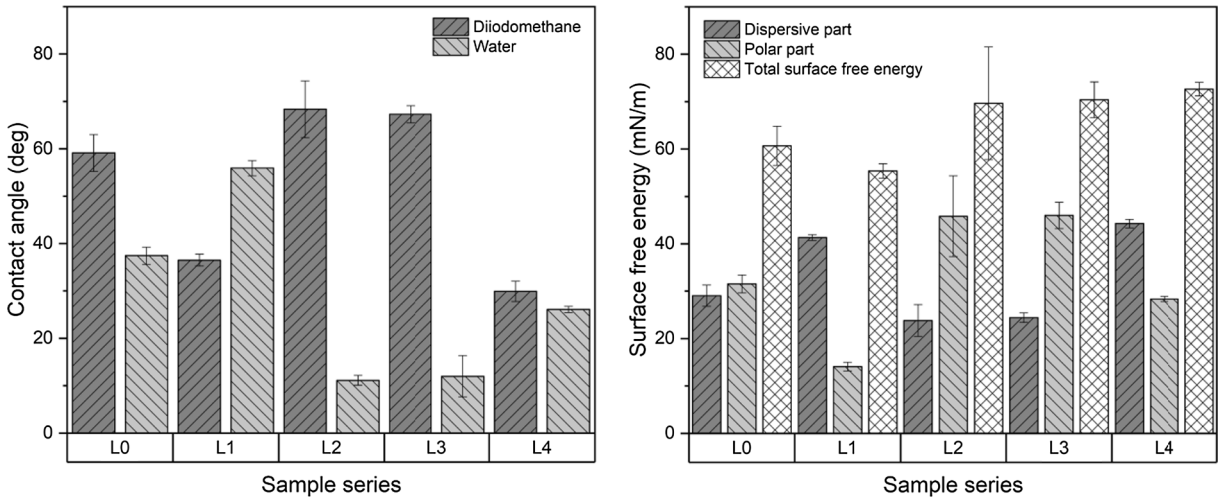

Fig. 5. Contact angle measurements for L0–L4 series (left) and corresponding SFE values with polar and dispersive contributions obtained by OWRK model (right).

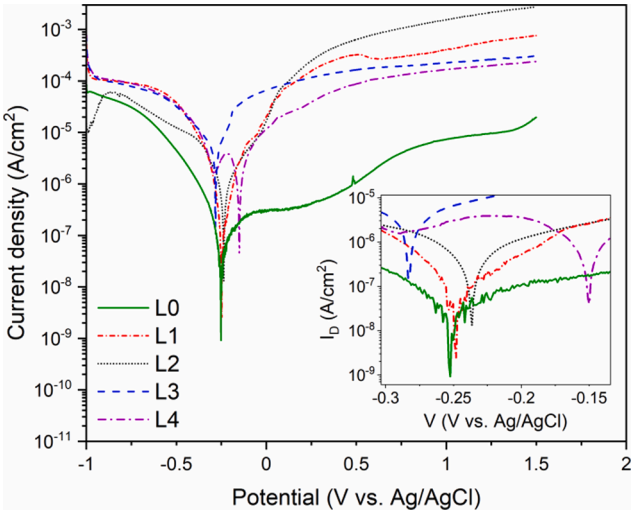

Fig. 6. Potentiodynamic polarization curves of reference sample (L0, straight line) and modified samples: chemically and plasma treated (L1, short dash-dotted line), CS (L2, dotted line), CS/Au NPs (L3, dash-dotted line) and CS/Ag NPs/Vit.C deposited (L4, dashed line).

with little deviation (−0.250V, $6.10 \cdot 10^{-9}$ A/cm^2 for L0, −0.248V, $2.44 \cdot 10^{-9}$ A/cm^2 for L1 and −0.236V, $1.31 \cdot 10^{-8}$ A/cm^2 for L2 sample), signifying little to no change in corrosion resistance compared to pure Ti6Al7Nb alloy. On the other hand, addition of noble metal nanoparticles seemed to slightly change the corrosion potential (−0.283V for Au NPs and −0.150V for Ag NPs containing sample), what is more registered current density has risen by few orders of magnitude for Au NPs modification ($1.43 \cdot 10^{-7}$ A/cm^2). No significant, corrosion related changes were revealed by the SEM micrographs done after LSV measurements, therefore they are not presented here. It should be noticed that on surface modified samples, higher cathodic current densities were registered. Therefore, it can be stated that the cathodic oxygen reduction (reaction (1)) proceeds more easily on samples of the titanium alloy whose surface has been modified.

$$O_2 + 2H_2O + 4e^- \rightarrow 4OH^- \quad (1)$$

In the anodic branch, the current density is around two orders of magnitude higher for the specimens of Ti6Al7Nb alloy covered by the chitosan based coatings. Considering these four coatings, the best corrosion resistance exhibits the specimen L4 (chitosan modified by Ag NPs).

Corrosion behaviour is an important aspect of metallic implants long term stability and safety, as dissolution of elements, which alloy consist of, may cause tissue irritation and long term toxicity. The investigation of corrosion potential *via* LSV showed no substantial change in both corrosion potential and current density for both etched (L1) and CS covered (L2) samples (Fig. 6), compared to already quite corrosion resistant Ti6Al7Nb alloy. On the other hand, the introduction of noble metal nanoparticles into chitosan layers induced a slight change of potential (lower in case of Au NPs and higher for Ag NPs) and raised corrosion current. However, no major rise of Ti, Al or Nb ion concentration in Ringer solution could be detected by ICP-MS measurement after 96h (Table 3). Given short times of the experiment, relative to the expected implant performance, more extensive study is needed to fully confirm or deny possible concerns.

3.4. Mechanical testing

Mechanical properties of deposited chitosan layers were evaluated in comparison with pure alloy as well as chemically and plasma treated surfaces. Nanoindentation method was deployed to acquire data in two loading regimes (see paragraph 2.2.6., Materials and methods section). Collected data was used to determine Young's modulus and hardness of layers by Oliver-Pharr method (Fig. 7 and Fig. S2, Supplementary Material).

Unfortunately, the E_{IT} and H_{IT} values were too high to consider a successful description of chitosan layers alone, but rather the data represents mechanical properties of near-surface region with all its elements combined. Nevertheless significant Young's modulus decrease can be noticed in low load regime for L2 sample, before reaching stable value after 200 mN measurement. The similar decrease in hardness can be seen for L3 and L4 samples, once again becoming similar in value to other samples after 200 mN measurement. The sudden drop in both E and H values for L1 sample at 400 mN load and L2 sample at 600 mN load is probably a result of a random void in the surface region and should not be taken into consideration. Patel *et al.* [57] reports Young's modulus values increase from 3.04 GPa for pure chitosan layer up to 5.22 GPa for Au NPs reinforced chitosan layers. Similar strengthening by nanoparticles was reported by Mishra *et al.* [58], who recorded values of Young's modulus between 4.8 and 6.6 GPa for chitosan-polyvinyl alcohol-silver nanocomposites, compared to 3.6 GPa for pure chitosan layer. Moreover, our study proved deterioration of those values in hydrated state for all deposited layers.

Additional data, regarding mechanical properties of deposited layers, was collected during scratch test conducted in progressive load mode (max. load 5N). Penetration depth of probed surfaces was comparable for L1 and L2 series (4.56 ± 0.71 μm and 4.46 ± 0.42 μm respectively) and exceed 5 μm for CS-based layers up to 5.84 ± 0.17 μm for L4 series (Fig. S3, Supplementary Material). Obtained results led to total loss of adhesion of brittle TiO_2 layer obtained during oxygen plasma treatment (L1), in contrast with only partial delamination of ductile polymer layers (L2–L4) – Fig. 8.

Such results should not be a surprise given the difference in chemical nature of layers and higher thickness of chitosan layers that received the same plasma pre-treatment as L1 modification. Besides qualitative state of the surface, scratch test provided quantitative data regarding the average coefficient of friction values as well as average friction force (Fig. 9).

Table 3
ICP-MS analysis of titanium, aluminium, niobium, gold and silver ions in DMEM collected after 48 h and 96 h cell treatment with substrates.

Ion type	Immersion time	Concentration (mg/dm^3)				
		L0	L1	L2	L3	L4
Ti	48 h	<0.0001	0.00034	<0.0001	0.00028	<0.0001
	96 h	<0.0001	<0.0001	0.00025	0.00029	<0.0001
Al	48 h	<0.002	<0.002	<0.002	<0.002	<0.002
	96 h	<0.002	<0.002	<0.002	<0.002	<0.002
Nb	48 h	<0.002	<0.002	<0.002	<0.002	<0.002
	96 h	<0.002	<0.002	<0.002	<0.002	<0.002
Au	48 h	–	–	–	10.38751	–
	96 h	–	–	–	2.80361	–
Ag	48 h	–	–	–	–	14.86204
	96 h	–	–	–	–	5.10672

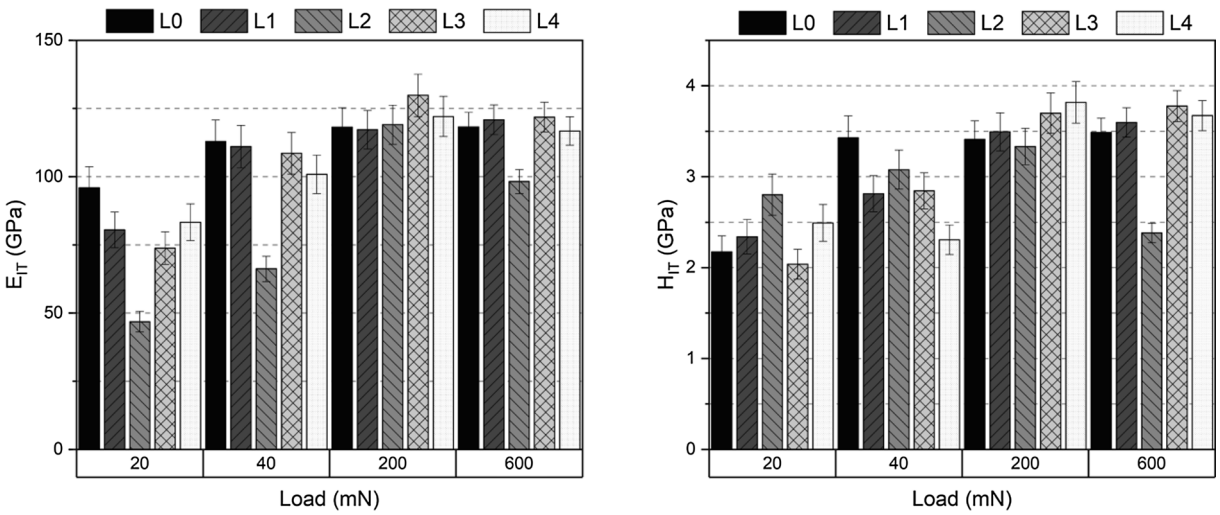

Fig. 7. Selected Young's modulus (left) and hardness (right) values of reference (L0) and modified (L1–L4) samples calculated from nanoindentation curves, using Oliver-Pharr method.

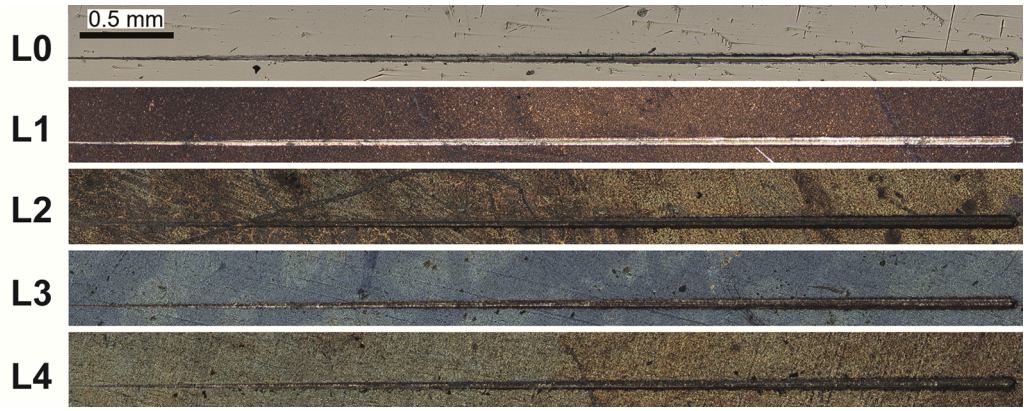

Fig. 8. Representative images of scratch test results for reference (L0) and modified samples (L1–L4).

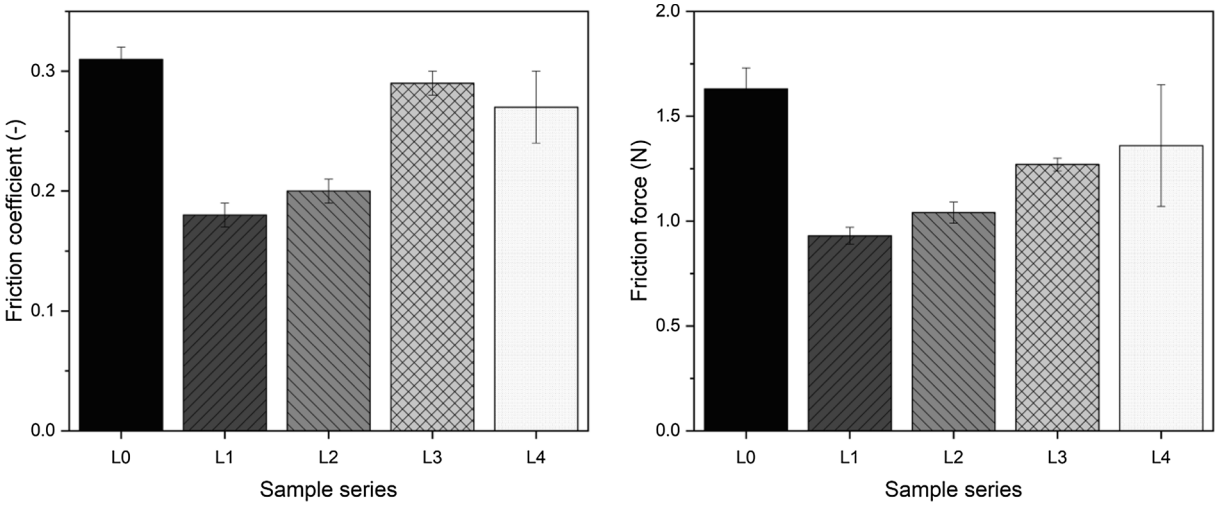

Fig. 9. The average coefficient of friction values (left) and average friction force (right) of tested samples for the applied load of 5N (L0–L4).

Determined coefficients of friction and friction forces revealed significant change in tribological behavior provided by plasma etching, as coefficient of friction value drops from 0.31 ± 0.01 for unmodified sample to 0.18 ± 0.01 for L1 sample. Friction force is also decreased in similar manner from 1.63 ± 0.10 N for L0 series to 0.93 ± 0.04 N for L1 series. Considering harmful effects of wear debris on patient health and implant longevity, proposed plasma modifications seem to bring benefits not only as a pre-treatment for further functionalization but also as

standalone modification in regions of implant exposed to friction. Understandably, deposition of chitosan layers (L2 series) caused coefficient of friction and friction force to increase (0.2 ± 0.01 and 1.04 ± 0.05N respectively), even more so for NPs enhanced layers (L3 and L4 series). Out of all modified samples CS/Au NPs layers displayed the highest friction coefficient (0.29 ± 0.01), while CS/Ag NPs layers reached the highest friction force (1.36 ± 0.29N). Despite rising values, none of them exceeded those for unmodified samples (L0), demonstrating overall improvement.

The interplay between mechanical properties of the implant material and osteoblast cells is important as biomechanical stimuli plays a major role in bone formation, modulating osteoblast gene expression [59]. Investigation of the mechanical properties of deposited chitosan-based layers, by nanoindentation, did not reveal information about layers itself, but rather about whole surface region spanning over few micrometres, which was obviously not the intention. Nevertheless, gathered data points out decrease of hardness and Young's modulus in near-surface region, which can be seen as positive effect, as materials used in implantology strive to imitate mechanical attributes of the human bone. The fact that true properties of chitosan layers were not discovered, given indentation depth (below 1 μm in low load regime), implies formation of thin layers, submicrometric in thickness. While this data might be helpful in assessing whether the proposed set of modifications is justified from biomedical point of view, it does not provide complete insight. Measurements of soft, polymer layers using nanoindentation method were proven to be challenging and adequate improvement of methodology should be considered in future studies in order to gather complete information on CS layers mechanical properties. Scratch tests revealed the importance of plasma pre-treatment in regard to proper tribological performance of implant, by reducing friction coefficient by nearly 40%, compared to unmodified Ti6Al7Nb alloy. Superior tribological properties of plasma modified Ti6Al7Nb alloy are supported by the findings of Kim et al., who used Large Pulsed Electron Beam (LPEB) to expose alloy surface to nitrogen plasma and successfully enhance alloys wear resistance [60]. Preventing wear is necessary to avoid issues such as fretting corrosion or tissue inflammation, caused by produced debris.

3.5. *In vitro biological evaluation*

Safety of implanted medical devices is of utmost importance and is subjected to rigorous control and testing. This is especially important when biomaterials or their modifications contain nanomaterials as constituent elements. In this study, silver and gold in form of nanoparticles, used as main antibacterial agents in prepared layers may cause adverse effects on human cells, if these metal ions are released too rapidly or nanoparticles are not embedded firmly enough. Thus, to asses influence of the resulting layers on human osteoblast cells, *in vitro* study of cytotoxicity on MG-63 cell line was carried out. Viability of cells cultured on substrates was evaluated after 48 and 96h by Alamar Blue assay (Fig. 10).

All modified surfaces turned out not to cause significant cytotoxicity in contact with MG-63 cells *in vitro* when compared with unmodified Ti6Al7Nb alloy. For instance, determined decrease in viability has not exceeded 16% and 14% after 48h and 96h, respectively (difference between L4 and L0 samples in both cases). Importantly, none of the modified substrates exhibited cytotoxicity higher than 20%. Such minor toxicity is on an acceptable level in accordance with EN ISO 10993 standard [54], proving modified samples biocompatible. Moreover, based on these results, it can be concluded that the MG-63 cells are more prone to proliferate on CS (L2) and CS/Au NPs (L3) samples than to the other two modifications (L1: chemical and plasma treatment, L4: CS/Ag NPs/Vit.C).

Then, in order to clarify the viability of particular cell populations incubated on exact surfaces, flow cytometry measurements allowing determination of viable and dead (apoptotic, necrotic) cells, were performed. In detail, the cell populations were harvested after 96h incubation and stained to enable fluorescent detection and classification of alive, early or late apoptotic cells and necrotic cells (Fig. 11).

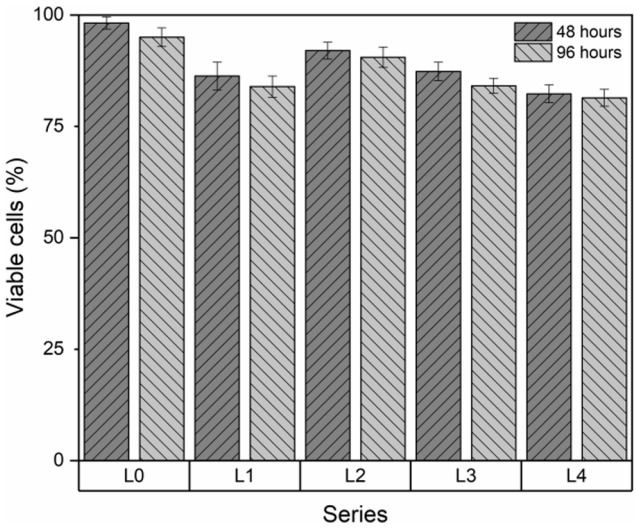

Fig. 10. MG-63 cells viability determined by Alamar Blue test for reference (L0) and modified Ti6Al7Nb samples (L1–L4) after 48h and 96h.

The results are in agreement with data obtained by Alamar Blue assay, which suggested slightly lower biocompatibility of L1 (chemical etching + plasma treatment) and L4 (CS/Ag NPs/Vit.C) surfaces. Those modifications seem to affect small population of MG-63 cells (percentages of necrotic cells: 3.9 ± 1.8% and 7.5 ± 1.3% for L1 and L4, respectively). In contrast to the above, pure CS and CS/Au NPs exhibited significantly less numerous populations (0.6 ± 0.2% and 0.9 ± 04% for L2 and L3, respectively). As well, populations of apoptotic, especially early apoptotic cells, for all modified samples (*ca.* 9% of total cell population for all L1-L4 series), are not considerably elevated. These results leave no doubt that the modified alloys meet the biocompatibility requirements.

To further investigate potential harmful ion release, affecting long term safety of the implant as well as to get insight into silver and gold ion release kinetics, ICP-MS study concerning major alloy components, Ag and Au was performed (Table 3).

Obtained results show a minimal release of Ti ions (concentrations

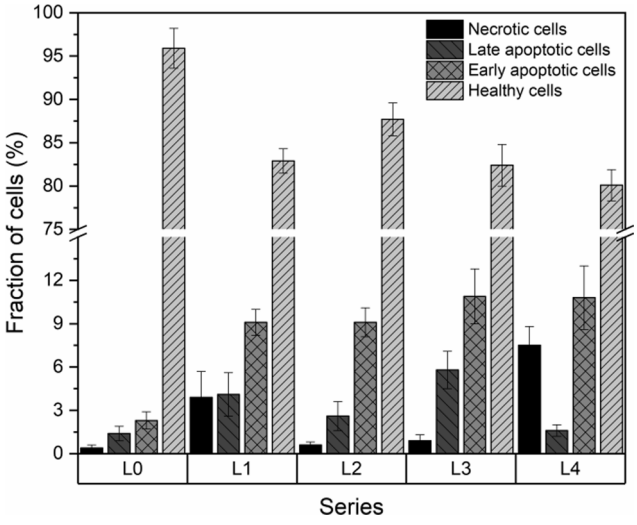

Fig. 11. Viable, early apoptotic, late apoptotic and necrotic cell populations cultured on reference (L0) and modified (L1–L4) samples, determined by flow cytometry.

below 1 μg/dm^3) for both immersion times (48h and 96h) and its alloying elements (concentrations below 2 μg/dm^3 for Al and Nb). This relation holds for all proposed modifications and reference sample with little fluctuation in time. More interesting release profile presents Au and Ag ions released from nanoparticles in the case of L3 (CS/Au NPs) and L4 (CS/Ag NPs/Vit.C) samples. While the initial concentrations are a quite high (over 10 mg/dm^3 for Au and over 14 mg/dm^3 for Ag ions after 48h), they tend to decay rather quickly just after another two days (nearly fourfold decrease for Au ions and nearly threefold for Ag ions after 96h). The observed "burst release" effect is a desirable phenomenon as it provides maximum anti-infection protection immediately after implantation. Inflammation is the normal physiological stage observed after implantation and accompanies its normal course. However, there is a fear of serious complications related to the development of bacterial infections, therefore the introduction of antibacterial components into surface modification of medical alloys with an explosive release kinetics at the beginning and then a slow release of reactive factors (sustained releasing) is the most optimal solution [13].

The results of biological evaluation provided optimistic answer to question of biocompatibility of manufactured layers. Alamar Blue test resulted in over 80% MG-63 cell viability for all four modifications, compared to unmodified sample, showing good tolerance of osteoblast-like cells towards applied layers with embedded nanoparticles (Fig. 10). Above-described results are in agreement with our other research regarding similar structures on NiTi [61]. In both studies, the main concern was brought by elevated levels of necrotic cells in case of chemically and plasma modified sample, as well as CS/Ag NPs/Vit.C layers. In the first modification it is possible, that cell death may be caused by oxidative stress, induced by residual reactive oxygen species after plasma treatment or adverse surface conditions. Moreover, in the case of Ag NPs containing layer ions release impact on slightly elevated cytotoxicity is presumable, as such effect was also shown in other studies [29]. Based on those remarks, care must be taken to optimise silver release profile in such a way that cell uptake will be minimised, while antibacterial effect will be retained. Gold and especially silver are well-known safe antibacterial agents, however, when provided with sufficiently controlled manner. Indeed, the incorporation of metal nanoparticles in the polymeric matrix or their direct surface modification with polymers significantly improve the biological effect – assure antibacterial mode of action while not cause cytotoxicity towards somatic mammalian cells. What is therefore absolutely important is prevention from an uncontrolled release of the metallic nanoparticles to the environment. Thus, such hybrid nanomaterials tune the bactericidal delivery of Ag or Au ions with a fast initial and subsequent sustained release at the infection site. Layers deposited in this study were characterised by continuous noble metal ion release up to 96h (Table 3). Various research reports the activity of Ag NPs and Au NPs against both Gram-positive and Gram-negative bacteria strains [28,31–33]. For instance, antimicrobial efficiency of cellulose fibers enriched with Ag NPs against different pathogens including bacteria and fungi (*Escherichia coli*, *Staphylococcus aureus*, *Candida albicans*, *Saccharomyces cerevisiae*) was proved by Ahmed *et al.* [39]. Then, Emam [40] demonstrated excellent antibacterial activity of Ag-Au bimetallic nanocomposites, obtained by eco-friendly method with application of natural arabinogalactan polysaccharide (Arabic gum). Very high antibacterial activity *in vitro* after 24h of incubation towards Gram-(-) and Gram-(+) bacteria strains was proved (up to 95.3–100% of bacterial reduction). Finally, provided in the current literature data suggest minimal inhibitive concentrations of Ag nanoparticles against two most common opportunistic bacteria: *E. coli* and *S. aureus* as 3.3 nM and 33 nM, respectively. Such concentrations are high enough to elicit bactericidal effect against most of bacteria strains responsible for implant-associated infections [62].

4. Conclusions

In this study multi-step modification of Ti6Al7Nb titanium alloy was successfully developed. Surface functionalisation based on chemical etching, O_2/NH_3/Ar plasma treatment and immersion deposition of chitosan layers embedded with Au NPs and Ag NPs induced significant changes to alloy surface. Usage of oxidative etching agents promoted growth of uniform, nanorough protective TiO_2 layer (S_a = 0.0937 μm and S_q = 0.1401 μm for L1 series). Plasma treatment resulted in improved tribological behaviour, indicated by decrease of friction coefficient from 0.31 for unmodified alloy (L0 series) to 0.18 for plasma etched samples (L1 series). Chitosan layers enhanced with nanoparticles of noble metals showed minimal toxicity towards MG-63 cell line *in vitro*. Favourably, highly hydrophilic surface state and release profile of silver and gold ions presumably assure sufficient antibacterial action and lack of significant cytotoxicity towards normal cells. Maintaining desired concentration of gold (2.80361 mg/dm^3 for L3 series) and silver (5.10672 mg/dm^3 for L4 series) ions up to 96h poise applied modifications to fight off biofilm formation. Moreover, achieving low contact angle value of 11.15° for L2 and 12.01° for L3 series adds to the anti-fouling effect. Furthermore, no major changes in corrosion behaviour and subsequent alloy-related ion release was observed. Positive evaluation of herein presented engineered surfaces may open a way to new solutions of tackling *peri*-implant infections and other bacteria related complications. Moreover, the usage of silver and gold as an alternative to antibiotics can hopefully help to battle a growing issue of antibiotic resistant bacteria.

CRediT authorship contribution statement

K. Kleszcz: Writing - original draft, Investigation, Formal analysis, Data curation. **M. Hebda:** Investigation, Formal analysis. **A. Kyzioł:** Investigation. **H. Krawiec:** Investigation. **K. Kyzioł:** Conceptualization, Methodology, Resources, Writing - review & editing, Supervision, Funding acquisition, Project administration.

Declaration of Competing Interest

The authors declare that they have no known competing financial interests or personal relationships that could have appeared to influence the work reported in this paper.

Acknowledgements

This work has been supported by the National Science Centre project (grant decision no. DEC-2017/01/X/ST8/00886) and the subsidy of the Ministry of Education and Science for the AGH University of Science and Technology in Kraków (Project No 16.16.160.557).

The authors thank to M. Migdalska, PhD for essential help in sample preparation. The authors also wish to express their gratitude to Victor Sebastian from University of Zaragoza (Department of Chemical Engineering, Aragon Institute of Nanoscience (INA), The Aragon Materials Science Institute (ICMA)) for carrying out TEM visualization. Finally, the authors thank to Joseph Anguiano for the linguistic correction of the manuscript.

Appendix A. Supplementary material

Supplementary data to this article can be found online at https://doi.org/10.1016/j.apsusc.2021.149795.

References

[1] M.C.S. Inacio, S.E. Graves, N.L. Pratt, E.E. Roughead, S. Nemes, Increase in total joint arthroplasty projected from to 2046 in Australia: a conservative local model with international implications, Clin. Orthop. Relat. Res. 475 (2017) (2014) 2130–2137, https://doi.org/10.1007/s11999-017-5377-7.

[2] M. Sloan, A. Premkumar, N.P. Sheth, Projected volume of primary total joint arthroplasty in the U.S to 2030, J. Bone Jt. Surg. 100 (2018) (2014) 1455–1460, https://doi.org/10.2106/JBJS.17.01617.

[3] V. Pilz, T. Hanstein, R. Skripitz, Projections of primary hip arthroplasty in Germany until 2040, Acta Orthop. 89 (2018) 308–313, https://doi.org/10.1080/17453674.2018.1446463.

[4] Y. Okazaki, E. Gotoh, Comparison of metal release from various metallic biomaterials in vitro, Biomaterials 26 (2005) 11–21, https://doi.org/10.1016/j.biomaterials.2004.02.005.

[5] B.C. Costa, C.K. Tokuhara, L.A. Rocha, R.C. Oliveira, P.N. Lisboa-Filho, J. Costa Pessoa, Vanadium ionic species from degradation of Ti-6Al-4V metallic implants: In vitro cytotoxicity and speciation evaluation, Mater. Sci. Eng. C. 96 (2019) 730–739, https://doi.org/10.1016/j.msec.2018.11.090.

[6] S. Höhn, S. Virtanen, Effect of inflammatory conditions and H 2 O 2 on bare and coated Ti-6Al-4V surfaces: corrosion behavior, metal ion release and Ca-P formation under long-term immersion in DMEM, Appl. Surf. Sci. 357 (2015) 101–111, https://doi.org/10.1016/j.apsusc.2015.08.261.

[7] M. Kaur, K. Singh, Review on titanium and titanium based alloys as biomaterials for orthopaedic applications, Mater. Sci. Eng. C. 102 (2019) 844–862, https://doi.org/10.1016/j.msec.2019.04.064.

[8] C. Exley, The toxicity of aluminium in humans, Morphologie 100 (2016) 51–55, https://doi.org/10.1016/j.morpho.2015.12.003.

[9] G.P. Rockwell, L.B. Lohstreter, J.R. Dahn, Fibrinogen and albumin adsorption on titanium nanoroughness gradients, Colloids Surf. B Biointerfaces 91 (2012) 90–96, https://doi.org/10.1016/j.colsurfb.2011.10.045.

[10] H.M. Wolford, K.M. Hatfield, P. Paul, S.H. Yi, R.B. Slayton, The projected burden of complex surgical site infections following hip and knee arthroplasties in adults in the United States through 2030, Infect. Control Hosp. Epidemiol. 39 (2018) (2020) 1189–1195, https://doi.org/10.1017/ice.2018.184.

[11] J. Gallo, M. Holinka, C. Moucha, Antibacterial surface treatment for orthopaedic implants, Int. J. Mol. Sci. 15 (2014) 13849–13880, https://doi.org/10.3390/ijms150813849.

[12] H. Chouirfa, H. Bouloussa, V. Migonney, C. Falentin-Daudré, Review of titanium surface modification techniques and coatings for antibacterial applications, Acta Biomater. 83 (2019) 37–54, https://doi.org/10.1016/j.actbio.2018.10.036.

[13] A. Kyzioł, W. Khan, V. Sebastian, K. Kyzioł, Tackling microbial infections and increasing resistance involving formulations based on antimicrobial polymers, Chem. Eng. J. 385 (2020), 123888, https://doi.org/10.1016/j.cej.2019.123888.

[14] K. Kyzioł, Ł. Kaczmarek, A. Kyzioł, Surface Functionalization of Biomaterials, John Wiley & Sons Inc, Hoboken, NJ, USA, 2017, pp. 457–490, https://doi.org/10.1002/9781119441632.ch80.

[15] C. Lüdecke, M. Roth, W. Yu, U. Horn, J. Bossert, K.D. Jandt, Nanorough titanium surfaces reduce adhesion of Escherichia coli and Staphylococcus aureus via nano adhesion points, Colloids Surf. B Biointerfaces. 145 (2016) 617–625, https://doi.org/10.1016/j.colsurfb.2016.05.049.

[16] F. Hizal, I. Zhuk, S. Sukhishvili, H.J. Busscher, H.C. van der Mei, C.-H. Choi, Impact of 3D hierarchical nanostructures on the antibacterial efficacy of a bacteria-triggered self-defensive antibiotic coating, ACS Appl. Mater. Interfaces. 7 (2015) 20304–20313, https://doi.org/10.1021/acsami.5b05947.

[17] T. Diu, N. Faruqui, T. Sjöström, B. Lamarre, H.F. Jenkinson, B. Su, M.G. Ryadnov, Cicada-inspired cell-instructive nanopatterned arrays, Sci. Rep. 4 (2015) 7122, https://doi.org/10.1038/srep07122.

[18] P.H. Chua, K.G. Neoh, Z. Shi, E.T. Kang, Structural stability and bioapplicability assessment of hyaluronic acid-chitosan polyelectrolyte multilayers on titanium substrates, J. Biomed. Mater. Res. Part A. 87A (2008) 1061–1074, https://doi.org/10.1002/jbm.a.31854.

[19] A. Kyzioł, K. Kyzioł, Surface functionalization with biopolymers via plasma-assisted surface grafting and plasma-induced graft polymerization—materials for biomedical applications, Biopolym. Grafting Appl., Elsevier (2018) 115–151, https://doi.org/10.1016/B978-0-12-810462-0.00004-1.

[20] Y. Wang, T. Wei, Y. Qu, Y. Zhou, Y. Zheng, C. Huang, Y. Zhang, Q. Yu, H. Chen, Smart, photothermally activated, antibacterial surfaces with thermally triggered bacteria-releasing properties, ACS Appl. Mater. Interfaces. 12 (2020) 21283–21291, https://doi.org/10.1021/acsami.9b17581.

[21] A. Tripathy, P. Sen, B. Su, W.H. Briscoe, Natural and bioinspired nanostructured bactericidal surfaces, Adv. Colloid Interface Sci. 248 (2017) 85–104, https://doi.org/10.1016/j.cis.2017.07.030.

[22] H. Lv, Z. Chen, X. Yang, L. Cen, X. Zhang, P. Gao, Layer-by-layer self-assembly of minocycline-loaded chitosan/alginate multilayer on titanium substrates to inhibit biofilm formation, J. Dent. 42 (2014) 1464–1472, https://doi.org/10.1016/j.jdent.2014.06.003.

[23] E. De Giglio, S. Cometa, M.A. Ricci, D. Cafagna, A.M. Savino, L. Sabbatini, M. Orciani, E. Ceci, L. Novello, G.M. Tantillo, M. Mattioli-Belmonte, Ciprofloxacin-modified electrosynthesized hydrogel coatings to prevent titanium-implant-associated infections, Acta Biomater. 7 (2011) 882–891, https://doi.org/10.1016/j.actbio.2010.07.030.

[24] J. Wang, J. Li, S. Qian, G. Guo, Q. Wang, J. Tang, H. Shen, X. Liu, X. Zhang, P. K. Chu, Antibacterial surface design of titanium-based biomaterials for enhanced bacteria-killing and cell-assisting functions against periprosthetic joint infection, ACS Appl. Mater. Interfaces. 8 (2016) 11162–11178, https://doi.org/10.1021/acsami.6b02803.

[25] H. Yazici, M.B. O'Neill, T. Kacar, B.R. Wilson, E.E. Oren, M. Sarikaya, C. Tamerler, Engineered chimeric peptides as antimicrobial surface coating agents toward infection-free implants, ACS Appl. Mater. Interfaces 8 (2016) 5070–5081, https://doi.org/10.1021/acsami.5b03697.

[26] M. D'Almeida, J. Amalric, C. Brunon, B. Grosgogeat, B. Toury, Relevant insight of surface characterization techniques to study covalent grafting of a biopolymer to titanium implant and its acidic resistance, Appl. Surf. Sci. 327 (2015) 296–306, https://doi.org/10.1016/j.apsusc.2014.11.185.

[27] M. Riaz, R. Zia, A. Ijaz, T. Hussain, M. Mohsin, A. Malik, Synthesis of monophasic Ag doped hydroxyapatite and evaluation of antibacterial activity, Mater. Sci. Eng. C. 90 (2018) 308–313, https://doi.org/10.1016/j.msec.2018.04.076.

[28] Z. Jia, P. Xiu, M. Li, X. Xu, Y. Shi, Y. Cheng, S. Wei, Y. Zheng, T. Xi, H. Cai, Z. Liu, Bioinspired anchoring AgNPs onto micro-nanoporous TiO2 orthopedic coatings: trap-killing of bacteria, surface-regulated osteoblast functions and host responses, Biomaterials 75 (2016) 203–222, https://doi.org/10.1016/j.biomaterials.2015.10.035.

[29] D. Bociaga, P. Komorowski, D. Batory, W. Szymanski, A. Olejnik, K. Jastrzebski, W. Jakubowski, Silver-doped nanocomposite carbon coatings (Ag-DLC) for biomedical applications – physiochemical and biological evaluation, Appl. Surf. Sci. 355 (2015) 388–397, https://doi.org/10.1016/j.apsusc.2015.07.117.

[30] M. Li, Y. Wang, L. Gao, Y. Sun, J. Wang, S. Qu, K. Duan, J. Weng, B. Feng, Porous titanium scaffold surfaces modified with silver loaded gelatin microspheres and their antibacterial behavior, Surf. Coatings Technol. 286 (2016) 140–147, https://doi.org/10.1016/j.surfcoat.2015.12.006.

[31] Y.F. Cheng, J.Y. Zhang, Y.B. Wang, C.M. Li, Z.S. Lu, X.F. Hu, L.Q. Xu, Deposition of catechol-functionalized chitosan and silver nanoparticles on biomedical titanium surfaces for antibacterial application, Mater. Sci. Eng. C. 98 (2019) 649–656, https://doi.org/10.1016/j.msec.2019.01.019.

[32] A. Regiel-Futyra, M. Kus-Liśkiewicz, V. Sebastian, S. Irusta, M. Arruebo, G. Stochel, A. Kyzioł, Development of noncytotoxic chitosan-gold nanocomposites as efficient antibacterial materials, ACS Appl. Mater. Interfaces. 7 (2015) 1087–1099, https://doi.org/10.1021/am508094e.

[33] A. Regiel-Futyra, M. Kus-Liśkiewicz, V. Sebastian, S. Irusta, M. Arruebo, A. Kyzioł, G. Stochel, Development of noncytotoxic silver–chitosan nanocomposites for efficient control of biofilm forming microbes, RSC Adv. 7 (2017) 52398–52413, https://doi.org/10.1039/C7RA08359A.

[34] D. Kadam, B. Momin, S. Palamthodi, S.S. Lele, Physicochemical and functional properties of chitosan-based nano-composite films incorporated with biogenic silver nanoparticles, Carbohydr. Polym. 211 (2019) 124–132, https://doi.org/10.1016/j.carbpol.2019.02.005.

[35] V. Amendola, M. Meneghetti, Laser ablation synthesis in solution and size manipulation of noble metal nanoparticles, Phys. Chem. Chem. Phys. 11 (2009) 3805–3821, https://doi.org/10.1039/b900654k.

[36] S. Ristig, D. Kozlova, W. Meyer-Zaika, M. Epple, An easy synthesis of autofluorescent alloyed silver-gold nanoparticles, J. Mater. Chem. B. 2 (2014) 7887–7895, https://doi.org/10.1039/c4tb01010h.

[37] H.E. Emam, H.B. Ahmed, Comparative study between homo-metallic & hetero-metallic nanostructures based agar in catalytic degradation of dyes, Int. J. Biol. Macromol. 138 (2019) 450–461, https://doi.org/10.1016/j.ijbiomac.2019.07.098.

[38] H.E. Emam, N.M. Saad, A.E.M. Abdallah, H.B. Ahmed, Acacia gum versus pectin in fabrication of catalytically active palladium nanoparticles for dye discoloration, Int. J. Biol. Macromol. 156 (2020) 829–840, https://doi.org/10.1016/j.ijbiomac.2020.04.018.

[39] H.B. Ahmed, H.E. Emam, H.M. Mashaly, M. Rehan, Nanosilver leverage on reactive dyeing of cellulose fibers: color shading, color fastness and biocidal potentials, Carbohydr. Polym. 186 (2018) 310–320, https://doi.org/10.1016/j.carbpol.2018.01.074.

[40] H.E. Emam, Arabic gum as bio-synthesizer for Ag–Au bimetallic nanocomposite using seed-mediated growth technique and its biological efficacy, J. Polym. Environ. 27 (2019) 210–223, https://doi.org/10.1007/s10924-018-1331-3.

[41] H.B. Ahmed, H.E. Emam, Synergistic catalysis of monometallic (Ag, Au, Pd)and bimetallic (Ag[sbnd]Au, Au[sbnd]Pd)versus trimetallic (Ag-Au-Pd)nanostructures effloresced via analogical techniques, J. Mol. Liq. 287 (2019), https://doi.org/10.1016/j.molliq.2019.110975.

[42] H.B. Ahmed, M.M. Mikhail, S. El-Sherbiny, K.S. Nagy, H.E. Emam, pH responsive intelligent nano-engineer of nanostructures applicable for discoloration of reactive dyes, J. Colloid Interface Sci. 561 (2020) 147–161, https://doi.org/10.1016/j.jcis.2019.11.060.

[43] P.J. Rivero, E. Ibañez, J. Goicoechea, A. Urrutia, I.R. Matias, F.J. Arregui, A self-referenced optical colorimetric sensor based on silver and gold nanoparticles for quantitative determination of hydrogen peroxide, Sensors Actuators B Chem. 251 (2017) 624–631, https://doi.org/10.1016/j.snb.2017.05.110.

[44] K. Sztandera, M. Gorzkiewicz, B. Klajnert-Maculewicz, Gold nanoparticles in cancer treatment, Mol. Pharm. 16 (2019) 1–23, https://doi.org/10.1021/acs.molpharmaceut.8b00810.

[45] M. Hoseinnejad, S.M. Jafari, I. Katouzian, Inorganic and metal nanoparticles and their antimicrobial activity in food packaging applications, Crit. Rev. Microbiol. 44 (2018) 161–181, https://doi.org/10.1080/1040841X.2017.1332001.

[46] W.C. Oliver, G.M. Pharr, An improved technique for determining hardness and elastic modulus using load and displacement sensing indentation experiments, J. Mater. Res. 7 (1992) 1564–1583, https://doi.org/10.1557/JMR.1992.1564.

[47] E. Vega-Avila, M.K. Pugsley, An overview of colorimetric assay methods used to assess survival or proliferation of mammalian cells, Proc. West. Pharmacol. Soc. 54 (2011) 10–14.

[48] A. Regiel, S. Irusta, A. Kyzioł, M. Arruebo, J. Santamaria, Preparation and characterization of chitosan–silver nanocomposite films and their antibacterial activity against *Staphylococcus aureus*, Nanotechnology. 24 (2013), 015101, https://doi.org/10.1088/0957-4484/24/1/015101.

[49] R.A. Mauricio-Sánchez, R. Salazar, J.G. Luna-Bárcenas, A. Mendoza-Galván, FTIR spectroscopy studies on the spontaneous neutralization of chitosan acetate films by moisture conditioning, Vib. Spectrosc. 94 (2018) 1–6, https://doi.org/10.1016/j.vibspec.2017.10.005.

[50] K.S.V. Krishna Rao, P. Ramasubba Reddy, Y.I. Lee, C. Kim, Synthesis and characterization of chitosan-PEG-Ag nanocomposites for antimicrobial application,

Carbohydr. Polym. 87 (2012) 920–925, https://doi.org/10.1016/j.carbpol.2011.07.028.
[51] D. Wei, W. Qian, Facile synthesis of Ag and Au nanoparticles utilizing chitosan as a mediator agent, Colloids Surf. B Biointerfaces 62 (2008) 136–142, https://doi.org/10.1016/j.colsurfb.2007.09.030.
[52] D.V. Nazarov, E.G. Zemtsova, A.Y. Solokhin, R.Z. Valiev, V.M. Smirnov, Modification of the surface topography and composition of ultrafine and coarse grained titanium by chemical etching, Nanomaterials. 7 (2017) 15, https://doi.org/10.3390/nano7010015.
[53] P. Solař, O. Kylián, A. Marek, M. Vandrovcová, L. Bačáková, J. Hanuš, J. Vyskočil, D. Slavínská, H. Biederman, Particles induced surface nanoroughness of titanium surface and its influence on adhesion of osteoblast-like MG-63 cells, Appl. Surf. Sci. 324 (2015) 99–105, https://doi.org/10.1016/j.apsusc.2014.10.082.
[54] K. Kyzioł, Ł. Kaczmarek, G. Brzezinka, A. Kyzioł, Structure, characterization and cytotoxicity study on plasma surface modified Ti–6Al–4V and γ-TiAl alloys, Chem. Eng. J. 240 (2014) 516–526, https://doi.org/10.1016/j.cej.2013.10.091.
[55] Y. Yuan, M.P. Hays, P.R. Hardwidge, J. Kim, Surface characteristics influencing bacterial adhesion to polymeric substrates, RSC Adv. 7 (2017) 14254–14261, https://doi.org/10.1039/C7RA01571B.
[56] X. Zhang, G. Zhang, H. Zhang, J. Li, X. Yao, B. Tang, Surface immobilization of heparin and chitosan on titanium to improve hemocompatibility and antibacterial activities, Colloids Surf. B Biointerfaces 172 (2018) 338–345, https://doi.org/10.1016/j.colsurfb.2018.08.060.
[57] N.G. Patel, A. Kumar, V.N. Jayawardana, C.D. Woodworth, P.A. Yuya, Fabrication, nanomechanical characterization, and cytocompatibility of gold-reinforced chitosan bio-nanocomposites, Mater. Sci. Eng. C. 44 (2014) 336–344, https://doi.org/10.1016/j.msec.2014.08.042.
[58] S.K. Mishra, J.M.F. Ferreira, S. Kannan, Mechanically stable antimicrobial chitosan–PVA–silver nanocomposite coatings deposited on titanium implants, Carbohydr. Polym. 121 (2015) 37–48, https://doi.org/10.1016/j.carbpol.2014.12.027.
[59] Y. Li, C. Ge, J.P. Long, D.L. Begun, J.A. Rodriguez, S.A. Goldstein, R.T. Franceschi, Biomechanical stimulation of osteoblast gene expression requires phosphorylation of the RUNX2 transcription factor, J. Bone Miner. Res. 27 (2012) 1263–1274, https://doi.org/10.1002/jbmr.1574.
[60] J. Kim, W.J. Lee, H.W. Park, Mechanical properties and corrosion behavior of the nitriding surface layer of Ti-6Al-7Nb using large pulsed electron beam (LPEB), J. Alloys Compd. 679 (2016) 138–148, https://doi.org/10.1016/j.jallcom.2016.04.060.
[61] P. Jabłoński, M. Hebda, P. Pytlak, A. Kyzioł, H. Krawiec, Z. Grzesik, K. Kyzioł, Impact of chitosan/noble metals-based coatings on the plasmochemically activated surface of NiTi alloy, Mater. Chem. Phys. 248 (2020), 122931, https://doi.org/10.1016/j.matchemphys.2020.122931.
[62] J.S. Kim, E. Kuk, K.N. Yu, J.-H. Kim, S.J. Park, H.J. Lee, S.H. Kim, Y.K. Park, Y. H. Park, C.-Y. Hwang, Y.-K. Kim, Y.-S. Lee, D.H. Jeong, M.-H. Cho, Antimicrobial effects of silver nanoparticles, Nanomed. Nanotechnol. Biol. Med. 3 (2007) 95–101, https://doi.org/10.1016/j.nano.2006.12.001.